# ULTRASONIC DETECTION OF CRACKS IN WEB GEOMETRIES

T. A. Gray and R. B. Thompson

Ames Laboratory, USDOE
Iowa State University
Ames, IA 50011

## INTRODUCTION

The need for high reliability interior crack detection in jet engine turbine components requires an optimal configuration of ultrasonic test equipment. Such optimization must be based upon the specific part geometries involved and upon the crack population which is supposed to exist in the parts. Due to the high cost with respect to time and manpower of fabrication, system evaluation and destructive analysis of experimental samples, it is preferable to simulate the detection process numerically in order to identify system configurations which promise high probability of detection of cracks. This paper describes such a computer model, presents experimental verification of its accuracy and illustrates its use in the design and optimization of ultrasonic detection systems for cracks in web geometries.

## DESCRIPTION OF DETECTION MODEL

For the purposes of this paper, detection is defined in terms of thresholding the amplitude of an ultrasonic signal in the presence of noise. Therefore, the detection model presented here computes signal-to-noise ratios by incorporating a model of the ultrasonic measurement process [1] and suitable models for various sources of noise. The purpose of the measurement model is to relate the far-field unbounded medium scattering amplitude of a flaw, A, to the actual measured ultrasonic signal, F, obtained in practice. This model can be expressed formally in the frequency domain as

$$F = R * T * D * P * A \qquad (1)$$

where R is a reference waveform taken, e.g., as the back-surface reflection from the test sample, T is a term which accounts for refraction and interface losses, D is a correction for diffraction effects, and P accounts for propagation losses (attenuation) and phase variation. A more detailed treatment of this model with a discussion of the associated errors and experimental confirmation for volumetric flaws can be found elsewhere [1].

For the detection simulations to follow, the scattering amplitude A in Eq. (1) was implemented as the elastodynamic Kirchhoff approximation to scattering from open flat elliptical cracks [2]. This scattering model was chosen over more exact theoretical results due to ease of implementation and computational speed. By way of illustration, Figs. 1 and 2 show comparisons between experimental and theoretical results for L→L backscatter from a circular crack. The experimental data were obtained from a laser-induced crack of radius 220μm in a thermoplastic resin sample [3]. The theoretical curves in these figures were obtained by using numerically exact results for smooth circular flat cracks obtained by the method of optimal truncation (MOOT) [4] and the Kirchoff approximation for the scattering amplitude A in Eq. 1. Comparisons of the scattering amplitudes themselves are found elsewhere [5]. Figure 1 shows the simulated and experimental amplitude spectra (magnitude of Eq. 1) and corresponding time domain signals (IFT of Eq. 1) for an incident angle of 30° relative to the crack normal and Fig. 2 shows the similar results for 60° incidence. The close correspondence between the MOOT and experimental results indicates both the accuracy of the measurement model and the near ideal nature of the crack in the lab sample. In addition, the curves corresponding to the Kirchhoff approximation are quite close to the exact and experimental data in terms of overall amplitude which indicates the applicability of this simple theory to threshold-type detection schemes. Of course, the Kirchhoff approximation predicts zero scattering at edge-on incidence to a crack, which is not borne out by either exact theoretical [4] or experimental [5] evidence. However, a typical detection configuration will be designed for illumination at incident angles nearer to normal.

To complete the detection model, the effects of measurement noise must be considered. At present, only coherent noise due to material inhomogeneities (e.g., pores) and incoherent receiver noise are incorporated in the detection model. Other noise sources, e.g., from spurious reflections, are not included. The variance of the coherent noise is computed by analysis similar to that used to develop the measurement model and by approximating the ultrasonic beam as a Gaussian profile. This variance is expressed as

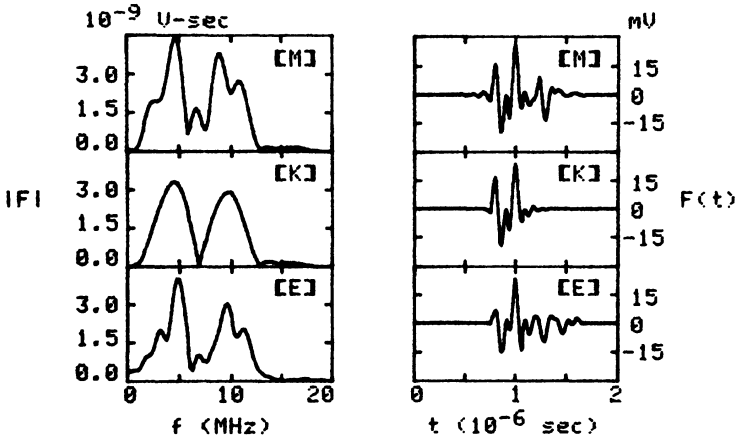


Fig. 1. Comparison of theoretical and experimental frequency and time domain signals from a circular crack ($a_F$=0.022cm) in thermoplastic sample at 30° illumination angle (M=MOOT, K=Kirchhoff, E=Experiment).

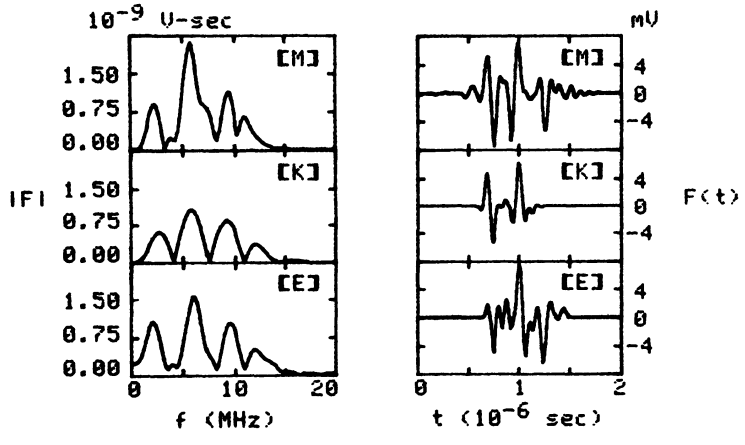


Fig. 2. Comparison of theoretical and experimental frequency and time domain signals from a circular crack ($a_F$=0.022cm) in thermoplastic sample at 60° illumination angle (M=MOOT, K=Kirchhoff, E=Experiment).

$$\sigma_c^2 = |R * T * D * P|^2 * |\bar{A}_2|^2 \omega^4 * N * \frac{v\tau}{2} \frac{\pi a^4}{w_x w_y} \qquad (2)$$

where R, T, D, and P have the same formal meaning as in Eq. (1), $|\bar{A}_2|^2\omega^4$ represents the mean Rayleigh scattering for the pores in the ultrasonic beam, N is the volume density of pores, and the remaining terms determine the volume of material interrogated by the beam where the beam widths $w_x$ and $w_y$ are computed according to transformation laws of Gaussian beams [5]. Further discussion of this model can be found in Ref. 8.

Receiver noise is modeled by the well-known approximation [6]

$$\sigma_E^2 = 4ktrb\eta \qquad (3)$$

where k = Boltzmann's constant, t is temperature (°K), r is receiver resistance (Ω), b is receiver bandwidth, and $\eta$ is a noise figure. The total RMS noise is taken to be $\sigma_c + \sigma_E$ and signal-to-noise ratios are defined to be the ratio of the maximum of the rectified RF flaw waveform to the total RMS noise.

In order to predict signal-to-noise ratios to be expected in an actual inspection application, the measurement and noise models must be calibrated to the transducers, inspected material properties and geometry, etc., in actual use. For the following simulations, calibration of the measurement and coherent noise models were effected by using an actual back-surface reflection signal from a 0.635 cm (0.25 in.) thick IN100 specimen for the reference signal R in Eqs. 1 and 2 and computing the diffraction terms D for the 0.635 cm (0.25 in.) diameter 10 MHz transducer used. In addition, the factor N in Eq. 2 was determined by fitting this equation to coherent noise data obtained from the IN100 specimen. The electronic noise model, eq. 3, was calibrated using characteristics of the receiver in use and fitting the noise figure $\eta$ to digitized receiver noise.

## PREDICTIONS FOR IN100

Predictions for backscatter from cracks in IN100 will be based upon the system and flaw parameters illustrated in Fig. 3. Of these quantities, the position and orientation of the transducer, $z_n$ and $\theta_T$, as well as the transducer radius and focal length may be considered to be system design parameters. The remaining variables shown in Fig. 3, which define the crack size, location, and orientation can be thought of as system evaluation parameters

to be used to test the utility of a proposed system design. This design/evaluation approach will be taken here.

It will be assumed that the crack population encountered in practice consists of circular cracks 0.02 cm to 0.2 cm in radius (16-160 mil diameters) with a preferred orientation perpendicular to the surface of the web (i.e., $\theta_F = \phi_F = 0$ in Fig. 3) with a possible angular deviation of $\pm 20^\circ$ and located 0.3175 cm (125 mil) from the surface of the plate which is 0.635 cm (250 mil) thick. Design of a detection system will be based upon the smallest crack ($a_F$ = .02 cm) in the preferred orientation ($\theta_F = \phi_F = 0$). Furthermore, measurements will be via mode converted T→T backscatter above the critical angle for L-waves in order to eliminate the L-wave mode.

Figure 4 shows simulated signal-to-noise ratios, S/N, for the nominal crack defined above as functions of the design parameters $\theta_T$ and $z_n$. In Fig. 4a (left hand plot) the variation in S/N versus $\theta_T$ is shown for various distances $z_n$ and Fig. 4b (right hand plot) shows S/N vs $z_n$ at various angles, $\theta_T$. Based on these graphs, a good candidate for the detection system is $\theta_T = 25^\circ$ and $z_n$ = 1.5 cm. Such design decisions are most appropriately based upon probability of detection (POD) analysis, of course, but the basic nature of design considerations is contained in the preceding arguments.

To illustrate use of the detection model to evaluate system configurations against various crack states, we can consider two such designs - a "standard" system, say $z_n$ = 10cm and $\theta_T = 18.8^\circ$ ($45^\circ$ in solid) and the "improved" configuration of the preceding paragraph. Figure 5 shows the variation of S/N due to $\pm 20^\circ$ deviations in the crack orientation angles $\theta_F$ and $\phi_F$ for these two system configurations assuming $a_F$ = 0.02cm. It is apparent that the improved configuration provides larger S/N than does the standard design for a given crack orientation. In practice, the results in Fig. 5 could also be instrumental in determining thresholds in order to detect misalligned cracks.

Two additional design parameters, the transducer radius and focal length, can also be considered. The detection model currently simulates signals from focussed transducers by assuming a Gaussian beam profile. Since no such transducers were available for experimental purposes, it was not possible to "calibrate" the model using an experimental reference waveform as discussed in the proceeding section. Therefore, the following results are not comparable in absolute terms to those in Figs. 4 and 5 but they do indicate the overall effects of focussing and transducer size. Figure 6 shows two such simulations. Figure 6a illustrates the improved S/N obtained using a focussed as compared to an unfocussed probe.

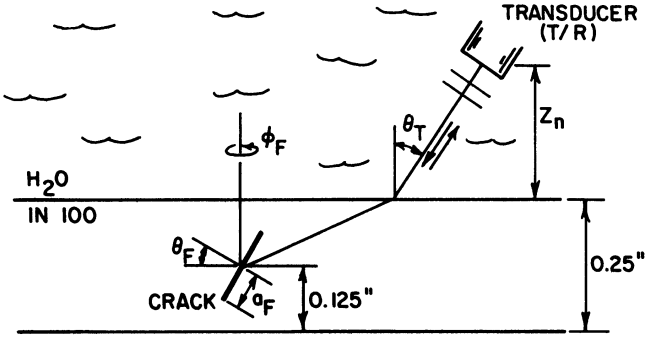


Fig. 3. Schematic representation of detection system and crack parameters used in simulation studies.

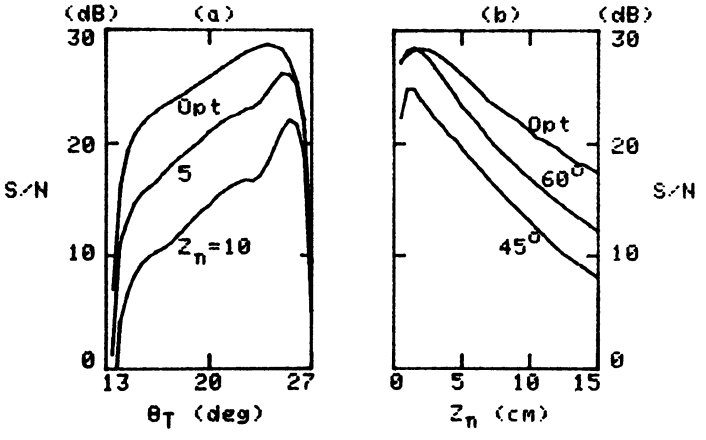


Fig. 4. Example of detection system design analysis. a) signal-to-noise versus transducer angle at various distances to sample. b) signal-to-noise versus separation distance at various transducer angles.

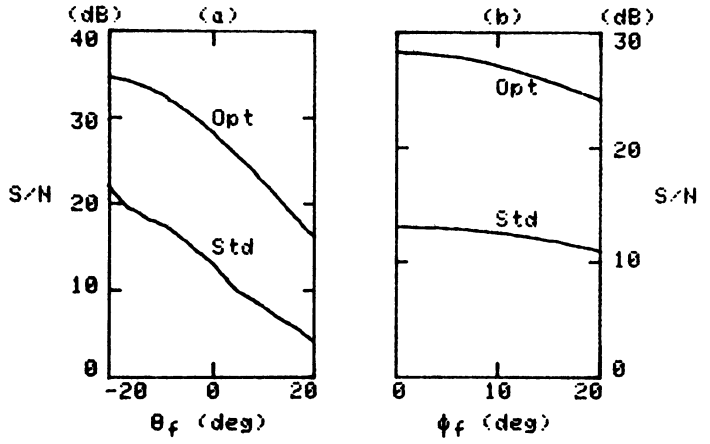


Fig. 5. Example of improved detectability using improved system configuration. a) signal-to-noise versus crack inclination. b) signal-to-noise versus crack azimuthal angle.

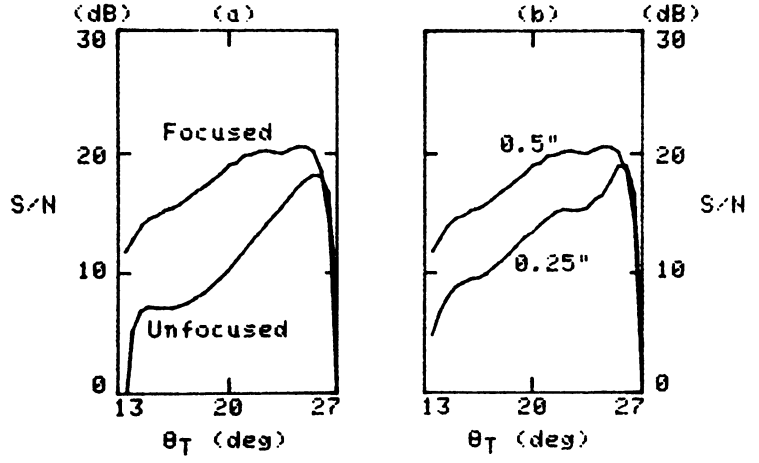


Fig. 6. Example of improved detectability using focussed transducers. a) signal-to-noise versus transducer angle for unfocussed and unfocussed probe. b) signal-to-noise versus transducer angle for focussed probes of different radii.

Similarly, Fig. 6b shows the improvement in S/N using wider aperture focussed probes due to smaller spot size.

## COMPARISON TO EXPERIMENT

A diffusion bonded IN100 plate, 0.635 cm (0.25 in.) thick was fabricated containing two semi-elliptical fatigue cracks normal to the bond plane in order to test the detection model against experimental data. The two cracks were designed to have roughly the same face area as circular cracks of radius 0.02 and 0.04cm (16 and 32 mil diam.), respectively, allowing for some closure during bonding. Figure 7 shows a comparison between experimental and model predicted S/N ratios for T→T backscatter as a function of transducer angle $\theta_T$. A crack radius of 0.04cm (0.032 in. diam.) was assumed for the model predictions. Experimental signal amplitudes were obtained by measuring the peak amplitude of the detected signal. Coherent RMS noise was estimated by computing the average of ten successive digitizations of a 1 microsecond time gate centered around the central plane of the IN100 plate at various positions along the sample.

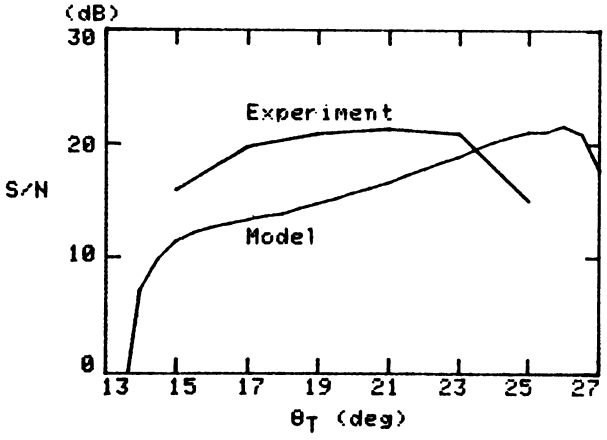


Fig. 7. Comparison between experimental and model simulated signal-to-noise versus transducer angle for fatigue crack in IN100 plate.

The lack of agreement between experimental and simulated results in Fig. 7 arises from several factors. First, the cracks in this sample were, in all probability, nearly closed. This speculation is based upon the observation that one crack in the sample was undetectable and the one which led to the data of Fig. 7 was detectable only from one side of the sample. This observation also supports the likelihood that the detected signals were corner reflections from the juncture of the crack opening with the diffusion bond plane. Such reflection would occur from only one side of the plate. Clearly, the simplified nature of the Kirchhoff approximation is inadequate to describe such scattering phenomena.

## DISCUSSION

The use of numerical modeling of the ultrasonic measurement process has been found to provide accurate estimation of experimental signal amplitudes on an absolute basis for well characterized flaws and part geometries. Further work in this approach will be directed to incorporating more realistic flaw scattering information - e.g., partial closure and surface roughness of cracks - and appropriate modifications to the theory to include effects of roughness of part surfaces and noise due to surface reflections. Applications of detection simulation to automated ultrasonic inspection system design and evaluation will also take into consideration errors of allignment of the ultrasonic beam upon specific flaws caused by discrete scanning increments. Once such upgrades are in hand, the use of computer modeling should prove to be a viable alternative to experimental testing of ultrasonic inspection systems for application to detection of interior cracks.

## ACKNOWLEDGEMENT

This work was sponsored by the Center for Advanced Nondestructive Evaluation, operated by the Ames Laboratory, USDOE, for the Air Force Wright Aeronautical Laboratories/Materials Laboratory and the Defense Advanced Research Projects Agency under Contract No. W-7405-ENG-82 with Iowa State University.

## REFERENCES

1. R. B. Thompson and T. A. Gray, J. Acoust. Soc. Am., (1983).
2. L. Adler and J. D. Achenbach, J. Nond. Eval., 1, 87 (1980).
3. D. K. Hsu, C. Y. She and Y. Li, these proceedings.
4. J. L. Opsal, private communication.
5. R. B. Thompson and T. A. Gray, these proceedings.
6. W. P. Willis and M. A. Herlin, Thermodynamics and Statistical Mechanics, McGraw-Hill Book Co., Inc., New York, 1952.

7. B. R. Tittmann and L. A. Ahlberg, in, Review of Progress in Quantitative NDE, D. O. Thompson and D. E. Chimenti, Eds., Plenum Press, New York, 2 (1982).
8. T. A. Gray and R. B. Thompson, ibid.

DISCUSSION

R.C. Addison, Jr. (Rockwell International Science Center): This is maybe too detailed for this forum, but you were commenting on the lack of agreement with the IN100 sample versus the samples that were in the thermoplastic, and there was one other difference, and maybe you had dealt with this, I'm not sure. When you are going into the plastic, there is a considerably smaller refraction angle that you are dealing with and so any aberrations in your beam or smearing around of the beam are going to be much smaller than they would be in the metal, and did you deal with that explicitly or not?

T.A. Gray: In the plot where I showed the comparison of the two results in the IN100 and the thermoplastic, the top angle in the thermoplastic was the critical angle for longitudinal waves, so there are going to be aberrations there as well.

From the Floor: I can't tell the frequency and I can't tell from your theory what the frequency dependence is, but is this the optimum frequency?

R.B. Thompson (Ames Laboratory): I think you are asking what is the optimum frequency for the transducer to be selected. We will hear a lot more about that in the paper by K. Fertig. You are really asking the question how would be construct an optimum filter and frequency domain to get the best possible signal to noise.